

Super-Robust Superhydrophobic Concrete

Jinlong Song ^{a,b}, Danyang Zhao ^{a,b*}, Zhengjin Han ^a, Wei Xu ^c, Yao Lu ^d, Xin Liu ^a, Bo Liu ^c, Claire J. Carmalt ^d, Xu Deng ^e, Ivan P. Parkin ^{d*}

Received 00th January 20xx,
Accepted 00th January 20xx

DOI: 10.1039/x0xx00000x

www.rsc.org/

Steel reinforced concrete is often used in buildings, roads and bridges, however, freeze-thaw damage and steel corrosion pose threats to the strength of concrete. Furthermore, ice formation on concrete road-surfaces greatly increases injury and fatality rates. Superhydrophobic materials are promising candidates to alleviate those problems due to their anti-corrosion and anti-icing properties. However, the weak mechanical robustness of superhydrophobic surfaces makes them difficult to apply to concrete surfaces. Here we report a facile route to fabricate superhydrophobic concrete (S-concrete) via covering metal mesh and fluoroalkylsilane modification. Comparative robustness tests, including sandpaper abrasion, knife scratch and hammer beat, were performed on commercial superhydrophobic paint+adhesive coatings and our S-concrete, which indicated that our S-concrete had far superior surface mechanical durability. To illustrate the practical prospects, we performed further tests on the S-concrete, including artificial cold rain, freeze-thaw, and corrosion under applied voltage in corrosive solution. The S-concrete showed remarkable anti-icing, anti-freeze-thaw, anti-corrosion properties, and mechanical robustness.

1. Introduction

Concrete, a mixture of cement as binder and aggregates as fillers, is widely used in most individual, commercial and public architecture because it has exceptional strength. However, its hydrophilic nature and porosity often reduce its surface mechanical durability and may even cause disasters. For example, in cold areas, the freeze-thaw of the trapped water in the pores of concrete causes expansion, cracking, scaling, and crumbing of road concrete ¹. The road ice formed from freezing rain and cold rain in a freezing environment creates nearly zero friction conditions for vehicle tires, increasing injury and fatality rates ². In coastal area, the corrosive Cl⁻ in seawater can corrode the steel bars used in concrete reinforcement, reducing strength and carrying capacity of sea bridges, flood control dams, and ports ³. The deposition of dirt and the colonization of concrete by microorganisms can deteriorate the aesthetics of buildings. Reducing the absorption of water is an effective approach to alleviate the aforementioned phenomenon and increase the mechanical durability of concrete in extreme harsh

environments. Superfine powders, e.g. silica fume ⁴, fly ash ⁵, slag ⁶, zeolite powder ⁷, and metakaolin powder ⁸, are often added in the concrete mixture to fill the gaps in the concrete and decrease the porosity to reduce the penetration speed and amount of water. Sealant coatings, such as an epoxy coating ⁹ or chlorinated rubber coating ¹⁰ are also used to cover the surface of concrete to isolate the concrete from water. Silane modification is also popular to make the concrete hydrophobic ¹¹. However, concrete that has added superfine powders is still superhydrophilic. Although the concrete covered with sealant coatings or modified with silane is hydrophobic, water still adheres to the surface and can easily form ice because of the high adhesive force between water and solid surface.

Recently, superhydrophobic surfaces with completely water-repellent properties have attracted increased attention for the protection of concrete ^{12, 13}. Superhydrophobicity is usually achieved by constructing micro rough structures and lowering the surface energy ¹⁴⁻¹⁷. Many techniques have been reported to fabricate non-wetting superhydrophobic surface including electrochemical etching ^{18, 19}, electrochemical deposition ^{20, 21}, chemical etching ²², chemical deposition ²³, laser etching ²⁴, thermal oxidation ²⁵, and coating ²⁶⁻²⁸ etc. Only coating based methods have been successful in endowing concrete surfaces with superhydrophobic properties ^{29, 30}. However, surface mechanical weakness is still the main problem that hinders the practical applications of superhydrophobic surfaces ³¹⁻³³. The micro-structures required for superhydrophobic surfaces are easily destroyed under mechanical wear ^{34, 35}. Obtaining a robust superhydrophobic surface on concrete is a key factor to promote the use of the superhydrophobic concrete (S-concrete).

^a Key Laboratory for Precision and Non-traditional Machining Technology of Ministry of Education, Dalian University of Technology, Dalian 116024, China. Email: zhaody@dlut.edu.cn

^b Collaborative Innovation Center of Major Machine Manufacturing in Liaoning, Dalian University of Technology, Dalian 116024, China.

^c School of Mechanics and Civil Engineering, China University of Mining and Technology (Beijing), 100083, China.

^d Materials Chemistry Research Centre, Department of Chemistry, University College London, 20 Gordon Street, London, WC1H 0AJ, UK. E-mail: i.p.parkin@ucl.ac.uk

^e Institute of Fundamental and Frontier Sciences, University of Electronic Science and Technology of China, Chengdu 610054, P. R. China.

Electronic Supplementary Information (ESI) available: [details of any supplementary information available should be included here]. See DOI: 10.1039/x0xx00000x

In this work, we developed a facile method to fabricate super-robust S-concrete by covering metal mesh and with additional fluoroalkylsilane modification in the base of the fabrication processes used for ordinary concrete. The surface robustness was characterized by sandpaper abrasion, knife scratch and even hammer beat and was greater than a well-known robust paint+adhesive coating^{34, 36}. The improvement of surface robustness was the result of the high hardness of the concrete and protection of the sand particles to fine-scale structures. With the help of induced superhydrophobicity, the S-concrete showed remarkable anti-icing, anti-freeze-thaw, anti-corrosion, and self-cleaning properties and has the potential to improve the life of many components of the built environment, especially roads in cold areas and bridges in coastal areas.

2. Experimental

2.1 Fabrication of super-robust S-concrete

100 g Portland cement (PO42.5) and 100 g sand (size < 250 μm) were put into a beaker and uniformly mixed. Then, 45 mL water and 0.6 g fluoroalkylsilane (FAS) were added into the beaker and stirred for 1 h with magnetic stirrer at 250 r/min to form a fresh concrete mixture. Cu meshes with wire size of 120 μm and pore size of 200 μm were used to cover the inner side wall and the bottom wall of a culture dish. Then, the fresh concrete mixture was poured into the culture dish and covered with Cu mesh at the top of concrete. After curing into rigid mass, the mesh was removed and S-concrete was obtained. The ordinary concrete (O-concrete) was fabricated using the same steps but without FAS and mesh.

2.2 Characterization

The morphologies of the samples were characterized using a scanning electron microscope (SEM, JSM-6360LV, Japan) at an accelerating voltage of 10 kV. The crystal structures were characterized using an X-ray diffractometer (XRD, Empyrean, Holland). The X-ray source was a $\text{CuK}\alpha$ radiation ($k = 0.15418$ nm), and was operated within the 5–80° range and at a scanning rate of $2\theta = 0.026$ °/min. The chemical compositions were characterized using an X-ray photoelectron spectroscopy (XPS, Thermo, ESCALAB 250Xi, USA). A monochromatic Al $\text{K}\alpha$ ($h\nu = 1486.6$ eV) was employed as X-rays source and C1s in hydrocarbon at binding energy of 284.6 eV was used as calibration reference. The diameter of the analyzed area was 500 μm . The pass energy and energy step of survey scans were respectively 100 eV and 1.0 eV, while those of C1s high-resolution spectra were respectively 30.0 eV and 0.1 eV. High-resolution C1s spectra were de-convoluted into different chemical groups with mixed Lorentzian–Gaussian components by XPSPeak v4.1 fitting software. A Shirley-type background subtraction was used and the full-width-at-half-maximum (FWHM) was fixed at 1.61 ± 0.26 eV. The wettability was characterized using an optical contact angle meter (Krüss, DSA100, Germany) by measuring the contact and sliding angles of water droplets with volume of 5 μL and 30 μL at ambient temperature. The dynamic bouncing processes of water droplets on the S-concrete was studied using a Phantom Fastcam SA5 high-speed camera (6000 frame/s). Water droplets

with volume of 9.5 μL were dropped from a height of 30 mm (tip to surface) using a micro-syringe at ambient temperature.

2.3 Surface mechanical robustness test

To show the super-robustness of the S-concrete, sandpaper abrasion, knife scratch and even hammer beat were used. To compare the surface mechanical durability between our S-concrete and a well-known robust superhydrophobic paint+adhesive coatings, we also performed the same robustness tests on commercial Never-wet spray coated O-concrete surfaces. Never-wet superhydrophobic coatings (S-coating) typically have high mechanical durability because an adhesive is used to improve the attraction between the coating and substrate. Never-wet S-coating were sprayed on the O-concrete according to product instructions. Figure S1(a) shows the schematic of sandpaper abrasion test, the samples were placed face-down to the sandpaper (sandpaper of 1500# and 360#) and abraded under a specific pressure (600 Pa and 1100 Pa). The water contact angles and sliding angles at different abrasion distance were characterized. Figure S1(b) shows the schematic of knife scratch, a knife was used to scratch the samples with movement perpendicular to the knife edge. Figure S1(c) shows the schematic of hammer beat, a hammer was used to beat the S-concrete to further show the super-robustness of the S-concrete. Sandpaper abrasion is a semi-quantitative test, whereas both knife scratch and hammer beat are the qualitative tests.

2.4 Anti-icing test

The S-concrete and O-concrete were positioned (the diameter of concrete was 6 cm, and the samples were tilted at an angle of 30°) into an environmental chamber (-5 °C) for the anti-icing tests, respectively. Artificial cold rain was then applied from a 5-pores nozzle onto the S-concrete and O-concrete surfaces. The rain temperature was 2.5 °C, the volume of single rain droplet was 13 μL , the impact velocity with concrete was 1 m/s, and the rainfall was at 3000 $\mu\text{L}/\text{min}$. Rain was stained for visualization.

2.5 Deicing force measurement

Smooth polyvinyl chloride (PVC) baffles were fixed as a box without top and bottom with size of $1.5 \times 1.5 \times 1.5$ cm^3 and put on the horizontal S-concrete and O-concrete of size $3 \times 3 \times 3$ cm^3 . Then, the cold rain with temperature of 2.5 °C was collected in the box in the environmental chamber (-5 °C). After 5 h, ice cube with size of $1.5 \times 1.5 \times 1.5$ cm^3 was formed and had a contact area of 1.5×1.5 cm^2 with the concrete. Then, the deicing force was measured by a force gauge (HP-100, Handpi Co.) at an environment temperature of 15 °C. Before measurement, the smooth PVC baffles were removed.

2.6 Anti-freeze-thaw-damage test

The freeze-thaw-damage was tested in a concrete freeze-thaw machine (KDS-28, Suzhou Donghua Test Equipment Co.) according to China national standard GB/T50082-2009. Before the accelerated freeze-thaw, the concrete cube samples with a size of $20 \times 20 \times 20$ mm^3 were immersed in water at temperatures of 18–22 °C for 4 days. Then the samples were put into the sample carrier that was filled with water and freeze-thawed

under from -18 to 10 °C with each cycle lasting 4 h. Before each weighing, the residue peeling off the samples was cleaned and the standing water on the sample surface was wiped by a wet towel. The mass loss was calculated as follows: $W_n = [(m_0 - m_n)/m_0] \times 100\%$, where W_n is the mass loss after n times of cycles, m_0 is the mass of original sample, m_n is the mass after n times of cycles. The ultrasonic velocity loss was tested by ultrasonic measuring instrument (RSM-SY8, Wuhan Zhongyan Technology Co.), the corresponding ultrasonic velocity loss was calculated as following: $D = [(V_n - V_0)/V_n] \times 100\%$, where D is the ultrasonic velocity loss, V_0 is the ultrasonic velocity in the original sample, V_n is the ultrasonic velocity in the sample after n times of cycles.

2.7 Anti-corrosion test

In this test, all electrochemical measurements were performed in 3.5 wt% aqueous NaCl solutions at room temperature using a computer-controlled potentiostat (Princeton Applied Research, VersaSTAT, USA) under open circuit conditions. For these electrochemical measurements, a three-electrode configuration, with a carbon steel bar coated with concrete (area, 8 cm²) as the working electrode, a platinum electrode as the counter electrode, and a saturated silver chloride electrode (SCE) as the reference electrode, were used. The thickness of concrete was 10 mm. The polarization curves were obtained at a sweep rate of 0.5 mV/s. The electrochemical impedance spectroscopy (EIS) measurements were conducted in the 100 mHz to 2 MHz frequency range using a 10 mV amplitude perturbation. To further study the anti-corrosion ability, the carbon steel bar coated with concrete was electrochemically corroded at 26 V for 20 s in 3.5 wt% aqueous NaCl solution. Then, the concrete was broken to observe the macro-morphology of the carbon steel bar. Before the test, all the samples were immersed in 3.5 wt% aqueous NaCl solutions for 24 h. We also tested the anti-corrosion property of double layer concrete composed of S-concrete and O-concrete (SO-concrete). The thickness of the S-concrete and O-concrete was 5 mm, respectively.

2.8 Compressive strength and flexural strength test

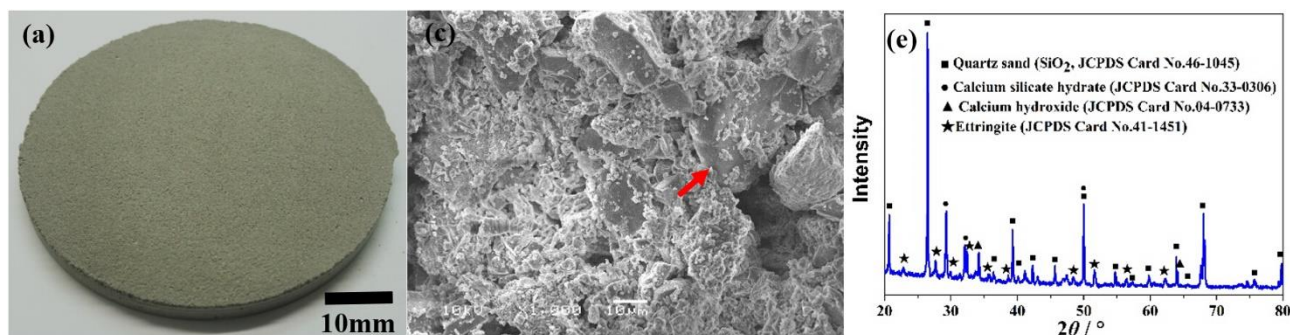
In this test, both the S-concrete and O-concrete were obtained by curing in room temperature for 3 days. The concrete cube samples with a size of 2×2×2 cm³ were compressed and destroyed by Pressure Tester (YA-2000, Shanghai Shuangxu Co.) to measure the compressive strength, as shown in Fig. S2(a).

The concrete beam with a size of 1.5×1.5×4.5 cm³ were bended by a force gauge (X206, Handpi Co.) to measure the flexural strength, as shown in Fig. S2(b).

3. Results and discussion

3.1 Surface morphology, chemical composition and superhydrophobicity

Figure 1 shows the surface morphology and chemical composition of the S-concrete. From the outside view, the S-concrete looks very similar to the traditional O-concrete, as shown in Figure 1(a) and Figure S3(a). However, at a micro-scale view, the whole surfaces of the S-concrete were divided into sub-millimeter convex shape structures with size of ca 200 μm with gullies with width of 120 μm, which was formed by the cover of Cu meshes, as shown in Figure 1(b). From the magnified view, the surface was composed of micro/nanometer-scale particles, and the naked quartz sand particles can be observed, as shown in Figure 1(c) and 1(d). For the O-concrete, there is no sub-millimeter convex shape structures but micro/nanometer-scale particles and no naked quartz sand particles are present, as shown in Figure S3(b) to S3(d). The XRD pattern indicates that the main composition of the S-concrete is quartz sand, calcium silicate hydrate, calcium hydroxide and ettringite, which is the same as O-concrete, as shown in Figure 1(e) and Figure S3(e). The nanometer-scale particles are calcium silicate hydrate, calcium hydroxide and ettringite, which come from the curing of Portland cement paste that binds the sand together^{37, 38}. In the XPS spectra, the peaks from F are not detected on the O-concrete but detected on the S-concrete, as shown in Figure S3(f). In addition, in the high-resolution C1s shown in Figure 1(f), the peaks from -CF₂ and -CF₃ groups were detected on the S-concrete, meaning the particles on the S-concrete were successfully coated with FAS. The existence of sub-millimeter, micro and nanometer-scale rough structures and low surface energy FAS make the S-concrete superhydrophobic. Water droplets on the S-concrete shows a typical globular shape, as shown in Figure 1(g). For 5 μL water droplet, the static contact angle was 156±0.8° and the sliding angle was only 6.1±1.2°. For 30 μL water droplet, the sliding angle was 5.4±1.2°. Such perfect superhydrophobicity make the dropped water droplet easily detach the concrete surface without any residue, showing a typical water bouncing processes, as shown in Figure 1(h) and Video S1. Thus, we have successfully transferred the concrete from a superhydrophilic to a superhydrophobic state.



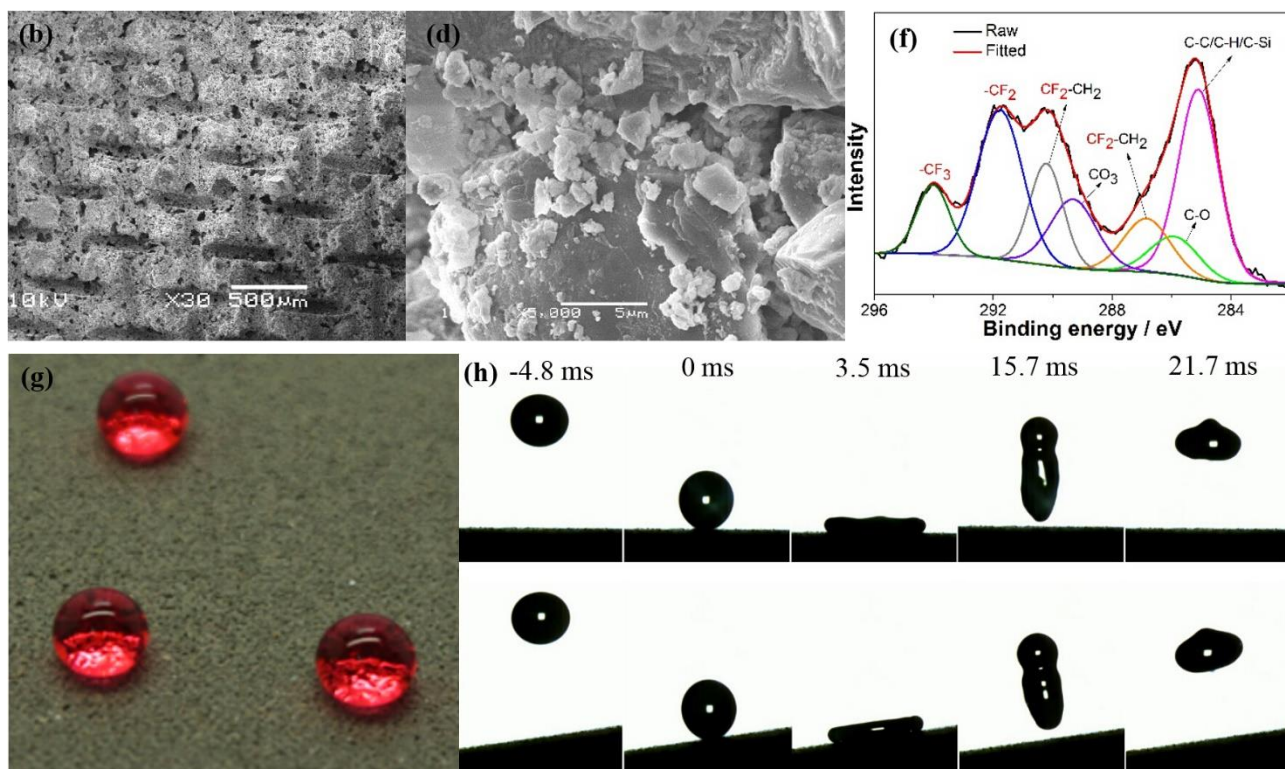
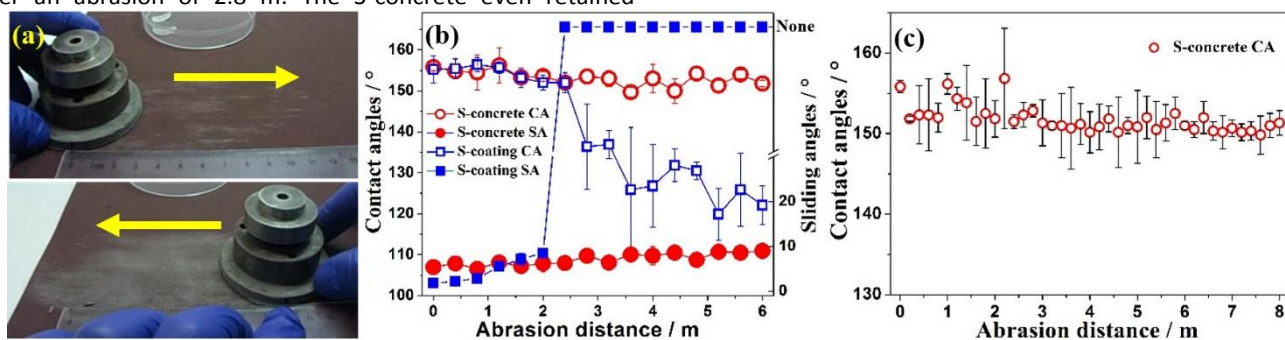


Figure 1. Surface morphology, chemical composition and superhydrophobicity of the S-concrete. (a) Macro digital photo. (b)-(d) SEM images with different magnifications (the arrow points to the sand). (e) XRD pattern. (f) The high-resolution XPS spectra of C. (g) Static photo of water droplets on the S-concrete (the water droplets are stained for visualization). (h) Dynamic bouncing processes of water droplets on the S-concrete (top: on the horizontal surface, bottom: on the gently sloping surface with tilting angle of 8°).

3.2 Surface mechanical robustness

A variety of methods were used to test the **surface** robustness of the S-concrete, including sandpaper abrasion, knife scratch, and hammer beat. A commercial superhydrophobic paint+adhesive coating (S-coating, Never-wet) was used to do the comparative test. For that coating, the adhesive was sprayed on the substrate to improve the robustness of the coating. The linear abrasion is shown in Figure 2(a). The S-concrete did not lose superhydrophobicity even if abraded for 6 m at the pressure of 600 Pa (standard sandpaper of 1500#), and still had a contact angle of $158 \pm 0.8^\circ$ and sliding angle of $9 \pm 1.2^\circ$, as shown in Figure 2(b). **The abraded surface was still rather rough than the O-concrete surface, as shown in Fig. S4.** However for the S-coating, there was no sliding angle for the abrasion of 2.4 m and the contact angle reduced to $136.4 \pm 10.4^\circ$ after an abrasion of 2.8 m. The S-concrete even retained

superhydrophobicity for pressure of 1100 Pa, standard sandpaper of 360#, and abrasion distance of 8 m, as shown in Figure 2(c) and Video S2. In the knife scratch test, when the scratch direction of the knife was perpendicular with the knife edge, the S-coating (especially the adhesive) was easily removed and the concrete lost superhydrophobicity, as shown in Figure 2(d) and Video S3. However, because of the high hardness of concrete and the protection of sand particles to fine-scale structures, the S-concrete still shows good superhydrophobicity after an equivalent scratch mode, as shown in Figure 2(e). Both the aforementioned two tests indicate that the S-concrete is more robust than the S-coating even though the latter used adhesive as a middle layer. Hence, we have termed the S-concrete super-robust. Finally, the hammer beat test also certified that the S-concrete was robust, as shown in Video S4.



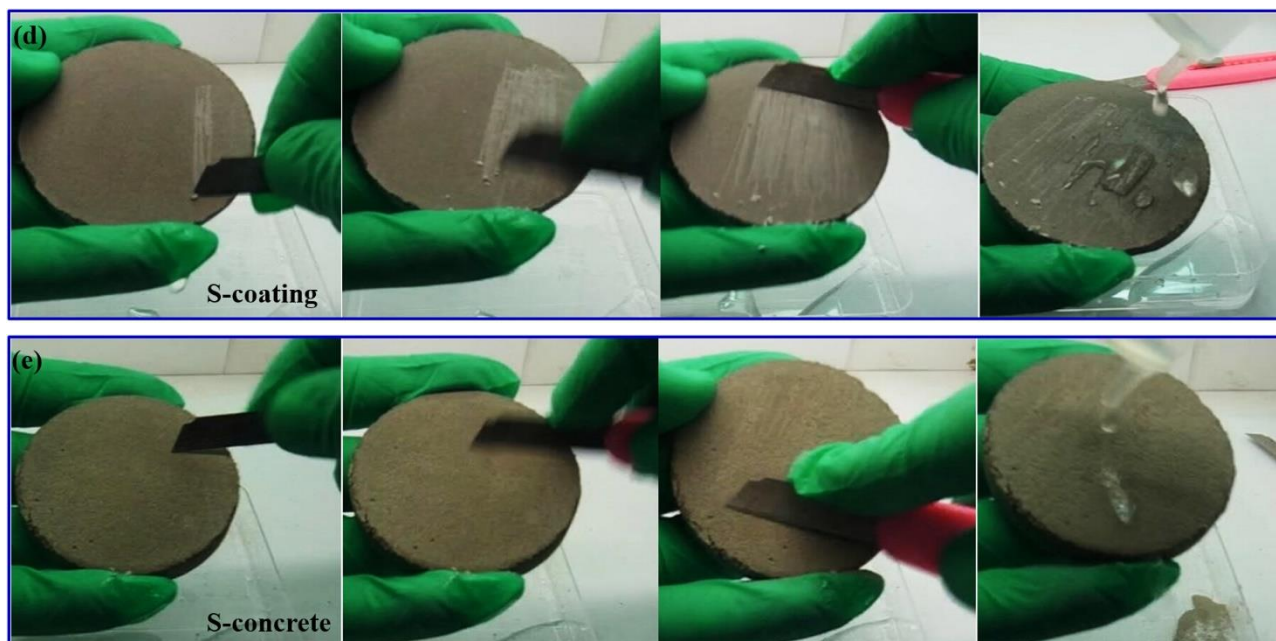


Figure 2. Robustness tests. (a) Sandpaper abrasion test processes with the samples facedown to the sandpaper. (b) The variation of contact angles and sliding angles with the abrasion distances under pressure of 600 Pa (standard sandpaper of 1500#) in the sandpaper abrasion test. (c) The variation of contact angles with the abrasion distances under pressure of 1100 Pa (standard sandpaper of 360#) in the sandpaper abrasion test, and the knife scratch on the O-concrete (d) and on the S-concrete (e). The volume of water droplets used in the measurement of contact angles and sliding angles are 5 μL and 30 μL , respectively.

3.3 Anti-icing, deicing from cold rain in freezing environment and anti-freeze-thaw-damage

Figure 3(a)-3(c) and Video S5 show the anti-icing property of the S-concrete compared with the O-concrete. For a rain temperature of 2.5 $^{\circ}\text{C}$ and environmental temperature of -5 $^{\circ}\text{C}$, the rain droplet easily adhered on the sloping O-concrete and froze into ice while rain droplets easily rolled off the sloping S-concrete without any residue. At a rainfall of 3000 $\mu\text{L}/\text{min}$ and raining time of 20 min, ice of 28.3 g was formed on the sloping O-concrete but no ice formed on the sloping S-concrete. In theory, the cold rain in freezing environment finds it difficult to adhere on the sloping S-concrete with a sloping angle larger than tilting angle of water droplet. For the horizontal concrete or the sloping concrete with sloping angle smaller than tilting angle, cold rain in freezing environment will stay on the surface and transfer into ice. However, the deicing force for the S-concrete is much lower than that for the O-concrete. Figure 3(d)-3(f) and Video S6 show the deicing experiment. For an ice cube with ice-concrete contact area of 1.5 \times 1.5 cm^2 , the ice on the O-concrete was difficult to remove and the deicing force was as high as 336.8 N and in addition, there was still residue ice on the surface. However, in the case of S-concrete, the ice was easily removed in whole without any residue with a deicing force was as small as 25.5 N which is reduced by a factor of more than 13 times compared with O-concrete. The perfect anti-icing property of the sloping S-concrete and low deicing force of the horizontal S-concrete from cold rain in the freezing environment would potentially reduce ice on the road in winter

and decrease injury and fatality rates, which result from low friction conditions between ice and vehicles.

We next tested the anti-freeze-thaw-damage ability of the S-concrete. The main reason for freeze-thaw-damage of the O-concrete is due to the expansion of volume of the absorbed water when transferred into ice, resulting in expansion, cracking, scaling, and crumbling which further shows mass loss and ultrasonic velocity loss. In our experiment, we found for the O-concrete, the mass loss increased with the number of freeze-thaw cycles and reached to 6.7% at 110 times of cycles, as shown in Figure 3(g). However, for the S-concrete, there was no mass loss observed after 130 times of freeze-thaw cycles and only 0.26% mass loss was seen after 190 times of cycles, hence showing an enhanced anti-freeze-thaw-damage ability. Similarly, the ultrasonic test showed that the ultrasonic velocity loss of the O-concrete was faster than that of the S-concrete with the number of freeze-thaw cycles, indicating the internal cracks and voids were not easily formed in the inside of the S-concrete under freeze-thaw, as shown in Figure 3(h). From the macro-morphology of concrete before and after freeze-thaw, we can see that the whole surface of the O-concrete was destroyed after 110 times of freeze-thaw cycles, while there were almost no change for the S-concrete after 210 times of freeze-thaw cycles, as shown in Figure 3(i). Therefore, the water-repellent property of the S-concrete could effectively decrease the absorbed water and the damage induced by freeze-thaw.

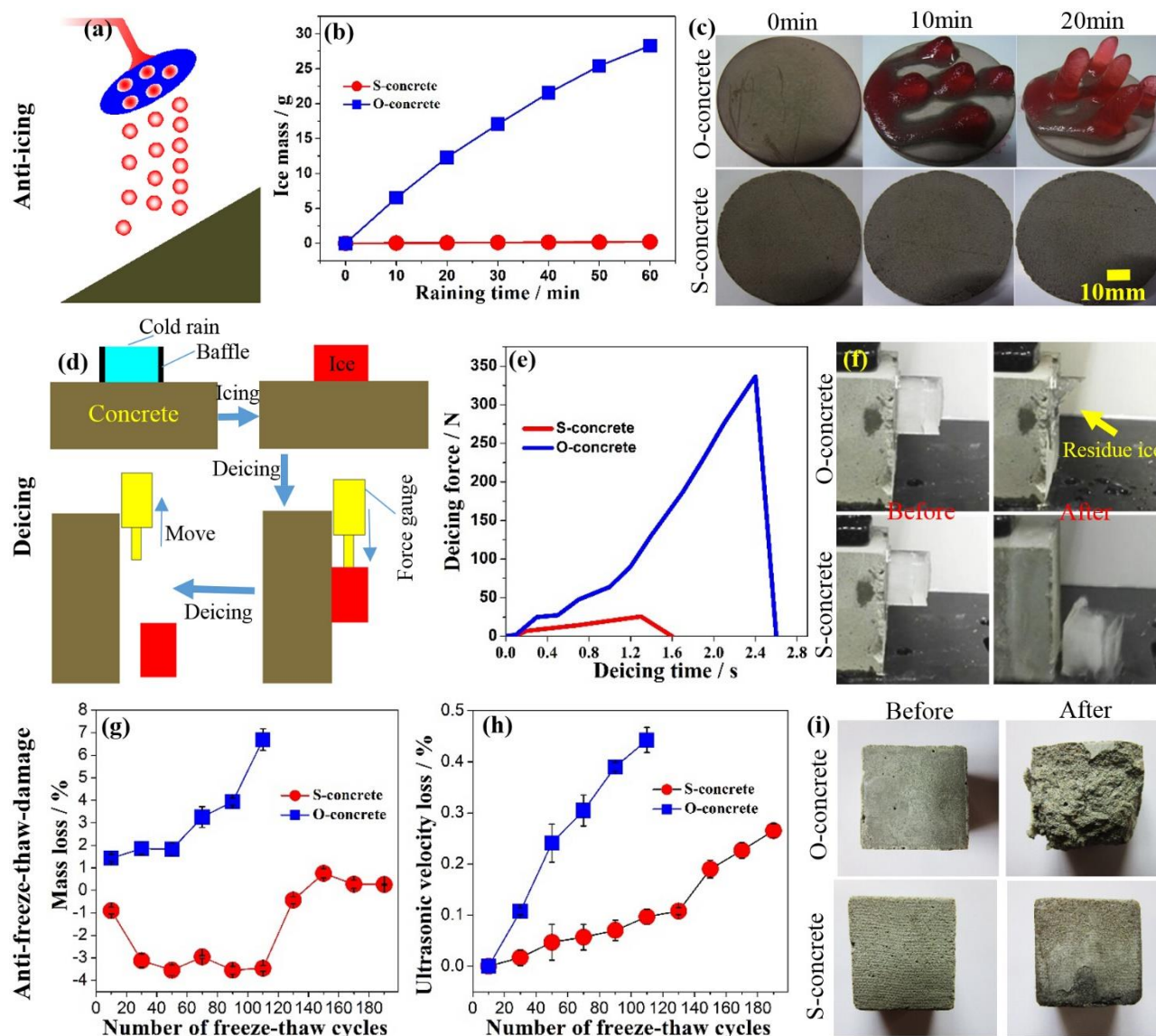


Figure 3. Anti-icing, deicing, and anti-freeze-thaw-damage of the S-concrete. (a) Schematic of raining of cold rain in the freezing environment. (b) The variation of ice mass with the raining time. (c) The macro-morphology of concrete after raining for 20 min (chamber temperature: $-5\text{ }^{\circ}\text{C}$; rain temperature: $2.5\text{ }^{\circ}\text{C}$; rain droplet: $13\text{ }\mu\text{L}$; impact velocity with concrete: 1 m/s ; rainfall: $3000\text{ }\mu\text{L/min}$; tilting angle of concrete: 30° . Rain was stained for visualization). (d) Schematic of the deicing experiment. Cold rain with temperature of $2.5\text{ }^{\circ}\text{C}$ was collected on the horizontal concrete surface by a PVC box without top and bottom and transferred into ice in the chamber with temperature of $-5\text{ }^{\circ}\text{C}$. The deicing force was measured by a force gauge at an environment temperature of $15\text{ }^{\circ}\text{C}$. (e) Deicing force of ice with ice-concrete contact area of 1.5 cm^2 on the concrete. (f) There was still residue ice on the O-concrete but no residue ice on the S-concrete after deicing processes. (g) The mass loss of the S-concrete and O-concrete with the number of freeze-thaw cycles. (h) The ultrasonic velocity loss of the S-concrete and O-concrete with the number of freeze-thaw cycles. (i) The micro-morphology of the concrete before freeze-thaw and after freeze-thaw for 110 times (O-concrete) and 210 times (S-concrete), sample size $20\times 20\times 20\text{ mm}^3$.

3.4 Anti-corrosion

The water-repellent property of the S-concrete can effectively prevent corrosive liquid from contacting with the steel bars for concrete reinforcement and improve the anti-corrosion ability of the steel bar. Figure 4(a) shows the samples of the carbon steel bars coated with concrete with thickness of 10 mm. In the potentiodynamic polarization curves shown in Figure 4(b), the corrosion potential and corrosion current density of carbon steel bars were -0.41 V and 2.61×10^{-7} A/cm² for the S-concrete and -0.65 V and 4.87×10^{-5} A/cm² for the O-concrete. The higher corrosion potential and lower corrosion current density of carbon steel bar in the S-concrete corresponds to a lower corrosion rate and a better corrosion resistance. Figure 4(c) shows the corresponding impedance which in the S-concrete is much higher than that in the O-concrete. The highly effective anti-corrosion ability can be seen on the macro-morphology of carbon steel bars under an applied voltage, as shown in Figure 4(d) and 4(e). After corrosion under 26 V voltage for 20 s in the 3.5 wt% NaCl aqueous solution, the whole steel surface coated with the O-concrete was corroded and covered with rust, while

the steel surface coated with the S-concrete was still very clean. Then, we also studied if S-concrete can protect the existing steel bar coated with the O-concrete. We next designed a double layer concrete composed of S-concrete and O-concrete (SO-concrete), as shown in Figure 2(f) and Figure S5. The carbon steel bar was coated with O-concrete inside and S-concrete outside. The corrosion potential and corrosion current density of carbon steel coated with the SO-concrete were -0.42 V and 4.31×10^{-6} A/cm², showing anti-corrosion. After corrosion under 26 V voltage for 20 s in the 3.5 wt% NaCl aqueous solution, the whole steel surface coated with SO-concrete was still very clean. This phenomenon indicates the S-concrete can protect the existing coastal concrete architecture. In summary, the use of the S-concrete may extend the service life of, for example sea bridges, flood control dam, and ports in coastal areas.

The S-concrete also has a good self-cleaning property. The CaCO₃ dirt on the S-concrete can be easily removed by artificial rain, as shown in Video S7.

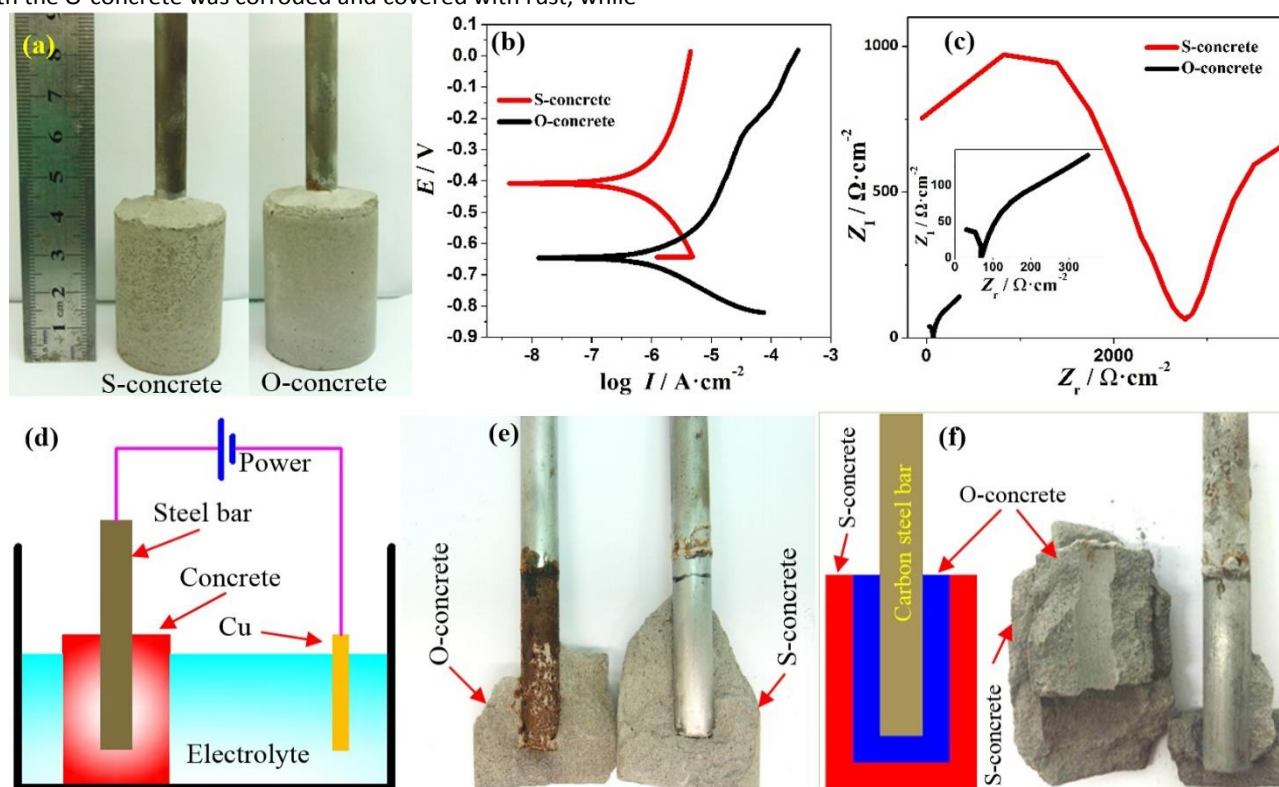


Figure 4. The protection of the steel bars for concrete reinforcement in the corrosion solution. (a) Carbon steel bar coated with the S-concrete and the O-concrete, respectively. The thickness of concrete is 10 mm. (b) The potentiodynamic polarization curves of the carbon steel bars coated with concrete in the 3.5 wt% NaCl aqueous solution. (c) The nyquist plots of the carbon steel bars coated with concrete in the 3.5 wt% NaCl aqueous solution. (d) The carbon steel bar and Cu plate was connected to the positive and negative polar of the power supply, respectively. Then, the carbon steel bars coated with S-concrete or O-concrete were electrochemically corroded under 26 V voltage for 20 s in the 3.5 wt% aqueous NaCl solution. (e) Macro-morphology of carbon steel bars coated with concrete after electrochemically corroded for 20 s under 26 V voltage in the 3.5 wt% NaCl aqueous solution. (f) Schematic of carbon steel bar coated with double layer concrete composed of S-concrete and O-concrete (SO-concrete) and macro-morphology of carbon steel bars coated with SO-concrete after electrochemically corroded for 20 s under 26 V voltage in the 3.5wt% NaCl aqueous solution. The thickness of the S-concrete and O-concrete was 5 mm, respectively. Before the corrosion, all the samples were immersed in the 3.5 wt% aqueous NaCl solutions for 24 h.

3.5 The influence of FAS

FAS, which contains the $-CF_3$ group with 6.7 mJ/m^2 surface energy and the $-CF_2-$ group with 18 mJ/m^2 surface energy could effectively reduce the surface energy of concrete. Fig. S6 shows the formation scheme of the self-assembled FAS film on concrete. The silicon ethoxide ($Si-OC_2H_5$) functional groups react with water to form silanols ($Si-OH$). Then, the silanols react with the $-OH$ groups on concrete particles which including quartz sand, calcium silicate hydrate, calcium hydroxide and ettringite to form a self-assembled film. Meanwhile, the silanols also induce vertical polymerization to form a grafted polysiloxane. All this guarantee that the concrete particles were covered with FAS. After curing into rigid mass, FAS distributed both in the outside and inside of the concrete. Fig. 5(a) shows the influence of FAS content on wettability of concrete obtained by Cu mesh covering. For 100 g cement, 100 g sand, and 45 g water, compared with the O-concrete, the adding of FAS improved the contact angle effectively while the FAS content

had little influence on the contact angle. However, the sliding angle was affected by FAS content largely. Only when the FAS mass was larger than 0.6 g, the superhydrophobicity with the contact angle larger than 150° and sliding angle smaller than 10° was obtained.

We next measured the compressive strength and flexural strength of concrete to study the influence of FAS on the strength of concrete. As shown in Fig. 5(b) and 5(c), the compressive strength and flexural strength of the O-concrete were 15.3 MPa and 3.9 MPa, respectively, while that of the S-concrete were 9.1 MPa and 2.6 MPa, respectively. The strength of the S-concrete was about 60% of that of the O-concrete. Thus, the adding of FAS will reduce the strength of concrete. However, for the practical application, we can enlarge the thickness of the S-concrete or construct the double layer concrete composed of outside S-concrete and inside O-concrete to improve the carrying capacity.

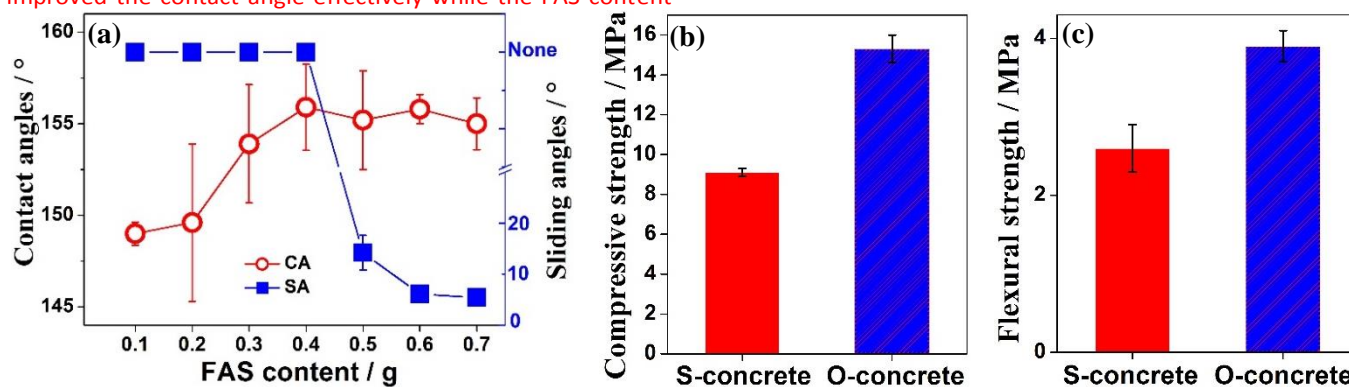


Figure 5. The Influence of FAS. (a) The influence of FAS content on wettability of concrete. The mass of cement, sand, and water are 100 g, 100 g, and 45 g, respectively. (b) The compressive strength of the S-concrete and O-concrete. (c) The flexural strength of the S-concrete and O-concrete.

Conclusions

In summary, this work demonstrates a simple method to fabricate super-robust superhydrophobic concrete (S-concrete). Sub-millimeter, micrometer, and nanometer structures coated with low surface energy FAS endow the superhydrophobicity with contact angles of $158 \pm 0.8^\circ$ and sliding angles of $6.1 \pm 1.2^\circ$. The S-concrete had a high surface robustness and retained superhydrophobicity under abrasion with 360# sandpaper and 1100 Pa pressure for 8 m distance. The S-concrete also had a good anti-knife scratch and anti-hammer beat ability. The high robustness is attributed to the high hardness of concrete and protection provided by sand particles to fine-scale structures from mechanical wear. The water-repellent property of the S-concrete endow the concrete with anti-ice properties from cold rain in a freezing environment, anti-freeze-thaw-damage, and helps prevent corrosive liquid from contacting with the steel bars for concrete reinforcement and helps improve the anti-corrosion ability of steel bar, and also shows self-cleaning effect. This kind of super-robust S-concrete has a large prospective application in the area of road concrete in cold areas and bridge concrete in coastal areas.

Acknowledgements

This project was financially supported by National Natural Science Foundation of China (NSFC, Grant No.51605078), Science Fund for Creative Research Groups of NSFC (51621064), and National Basic Research Program of China (Grant No.2015CB057304).

References

- W. Li, M. Pour-Ghaz, J. Castro, J. Weiss, *J. Mater. Civil. Eng.* 2012, **24**, 299.
- M. P. Andreescu, D. B. Frost, *Clim. Res.* 1998, **9**, 225.
- V. Maruthapandian, V. Saraswathy, S. Muralidharan, *Cement Concrete Comp.* 2016, **74**, 100.
- C. S. Poon, S. C. Kou, L. Lam, *Constr. Build. Mater.* 2006, **20**, 858.
- G. Li, *Cement Concrete Res.* 2004, **34**, 1043.
- T. Bakharev, J. G. Sanjayan, Y. B. Cheng, *Cement Concrete Res.* 2003, **33**, 1607.
- N. Feng, G. Peng, *Constr. Build. Mater.* 2005, **19**, 579.
- P. Dinakar, P. K. Sahoo, G. Sriram, *Int. J. Concr. Struct. M.* 2013, **7**, 215.

- 9 K. Saravanan, S. Sathiyarayanan, S. Muralidharan, S. S. Azim, G. Venkatachari, *Prog. Org. Coat.* 2007, **59**, 160.
- 10 A. A. Almusallam, F. M. Khan, S. U. Dulaijan, O. S. B. Al-Amoudi, *Cement Concrete Comp.* 2003, **25**, 473.
- 11 Y. Zhu, S. Kou, C. Poon, J. Dai, Q. Li, *Cement Concrete Comp.* 2013, **35**, 32.
- 12 T. M. Schutzius, S. Jung, T. Maitra, G. Graeber, M. Köhme, D. Poulidakos, *Nature* 2015, **527**, 82.
- 13 F. Xiao, S. Yuan, B. Liang, G. Li, S. O. Pehkonen, T. Zhang, *J. Mater. Chem. A* 2015, **3**, 4374.
- 14 X. Gao, L. Jiang, *Nature* 2004, **432**, 36.
- 15 T. Darmanin, E. T. de Givenchy, S. Amigoni, F. Guittard, *Adv. Mater.* 2013, **25**, 1378.
- 16 E. J. Falde, S. T. Yohe, Y. L. Colson, M. W. Grinstaff, *Biomaterials* 2016, **104**, 87.
- 17 B. Su, Y. Tian, L. Jiang, *J. Am. Chem. Soc.* 2016, **138**, 1727.
- 18 F. Xiao, S. Yuan, B. Liang, G. Li, S. O. Pehkonen, T. Zhang, *J. Mater. Chem. A* 2015, **3**, 4374.
- 19 W. Jiang, J. He, M. Mao, S. Yuan, H. Lu, B. Liang, *Ind. Eng. Chem. Res.* 2016, **55**, 5545.
- 20 N. Xu, D. K. Sarkar, X. Chen, W. P. Tong, *Surf. Coatings Technology* 2016, **302**, 173.
- 21 N. Wang, Y. Yuan, Y. Wu, T. Hang, M. Li, *Langmuir* 2015, **31**, 10807.
- 22 J. Guo, F. Yang, Z. Guo, *J. Colloid Interf. Sci.* 2016, **466**, 36.
- 23 J. Song, S. Huang, Y. Lu, X. Bu, J. E. Mates, A. Ghosh, R. Ganguly, C. J. Carmalt, I. P. Parkin, W. Xu, C. M. Megaridis, *ACS Appl. Mater. Inter.* 2014, **6**, 19858.
- 24 M. Tang, X. Huang, J. Yu, X. Li, Q. Zhang, *J. Mater. Process. Tech.* 2017, **239**, 178.
- 25 L. Li, T. Huang, J. Lei, J. He, L. Qu, P. Huang, W. Zhou, N. Li, F. Pan, *ACS Appl. Mater. Inter.* 2015, **7**, 1449.
- 26 W. Wang, K. Lockwood, L. M. Boyd, M. D. Davidson, S. Movafaghi, H. Vahabi, S. R. Khetani, A. K. Kota, *ACS Appl. Mater. Inter.* 2016, **8**, 18664.
- 27 M. J. Nine, M. A. Cole, L. Johnson, D. N. Tran, D. Losic, *ACS Appl. Mater. Inter.* 2015, **7**, 28482.
- 28 S. T. Yohe, M. W. Grinstaff, *Chem. Commun.* 2013, **49**, 804.
- 29 I. Flores-Vivian, V. Hejazi, M. I. Kozhukhova, M. Nosonovsky, K. Sobolev, *ACS Appl. Mater. Inter.* 2013, **5**, 13284.
- 30 S. W. Muzenski, I. Flores-Vivian, M. I. Kozhukhova, S. Rao, M. Nosonovsky, K. Sobolev, *Nanotechnology in Construction: Proceedings of NICOM5*, Springer, Germany 2015.
- 31 X. Tian, T. Verho, R. H. A. Ras, *Science* 2016, **352**, 142.
- 32 M. Cheng, S. Zhang, H. Dong, S. Han, H. Wei, F. Shi, *ACS Appl. Mater. Inter.* 2015, **7**, 4275.
- 33 R. M. Bar, S. Widmaier, P. A. Levkin, *RSC Adv.* 2016, **6**, 98257.
- 34 Y. Lu, S. Sathasivam, J. Song, C. R. Crick, C. J. Carmalt, I. P. Parkin, *Science* 2015, **347**, 1132.
- 35 L. B. Boinovich, A. G. Domantovskiy, A. M. Emelyanenko, A. S. Pashinin, A. A. Ionin, S. I. Kudryashov, P. N. Saltuganov, *ACS Appl. Mater. Inter.* 2014, **6**, 2080.
- 36 B. Chen, J. Qiu, E. Sakai, N. Kanazawa, R. Liang, H. Feng, *ACS Appl. Mater. Inter.* 2016, **8**, 17659.
- 37 M. Cheyrezy, V. Maret, L. Frouin, *Cement Concrete Res.* 1995, **25**, 1491.
- 38 M. K. Maroliya, *IOSR J. Eng.* 2012, **2**, 12.